2008-04-28

Diffusion and Phase Change During Heat Treatment of Ni-B Coatings on Steel

Kevin W. Shepardson
Worcester Polytechnic Institute

Diffusion and Phase Change During Heat Treatment of Ni-B Coatings on Steel

By

Kevin Shepardson

A Thesis

Submitted to the Faculty

of the

Worcester Polytechnic Institute

In partial fulfillment of the requirements for the

Degree of Master of Science

In

Materials Science and Engineering

April 2008

APPROVED:

_____

Richard D Sisson Jr., Advisor
George F. Fuller Professor
Materials Science and Engineering Program Head

Abstract

Nickel-boron coatings are used to improve friction and wear properties (and, in some cases, corrosion resistance). The nickel-boron coating investigated here is 5-6 wt% boron, and is deposited by electroless plating on a 1018 steel substrate. It is amorphous as-plated, and heat treatment is used to crystallize the coating to improve its hardness.

To better understand and predict the effects of heat treatment, samples that had been isothermally annealed at various temperatures from 500ºC to 800ºC for either 2h or 5h were examined by several methods to determine the diffusion effects taking place during annealing. Samples were examined by XRD, both at the coating surface and at multiple depths within the coating. Optical microscopy and SEM were used to view the structure of the coating in cross-section. Cross sections were etched and examined by optical microscopy and SEM, as well as EDS, which was used to develop a Ni-Fe composition profile at the coating-substrate interface. Microhardness measurements were taken and used to develop microhardness profiles. Additional samples were annealed to investigate boron oxidation at the coating surface.

Based on the data, there is a reduced amount of Ni_3B near the outer surface of the heat-treated coatings, with the thickness of the resultant γ-Ni layer increasing with annealing time and temperature, from 2.4 to just over 13 μm. This low-boron region indicates that boron is diffusing out through the surface of the coating and oxidizing, which the literature indicates should result in the formation of B_2O_3. Because B_2O_3 is water-soluble, it is likely that it dissolved during the water quench that concluded most anneals. Diffraction and EDS data also indicate interdiffusion of the nickel in the coating and the iron in the steel substrate. This leads to the formation of a soft interdiffusion

layer between the Ni_3B coating bulk and steel substrate that appears to be a mix of ferrite and Ni_3Fe.

Table of Contents

List of Numbered Figures

List of Numbered Tables

1. Introduction

UltraCem™, produced by UCT Coatings, Inc., is an electroless nickel-boron coating containing approximately 5-6 wt% boron [1]. It is used as a wear-resistant coating, due to its high hardness. When heat-treated under certain conditions, hardness values as high as 1400 on the Knoop (25gf, 10s) scale have been reported [2]. Heat treatment is necessary because the electroless plating process used deposits a mostly amorphous coating, which has a lower hardness than heat-treated coatings.[Riddle and Bailer]

Previous work [2][3] has examined the relationship between heat treatment and coating properties, and determined that phase transformations take place during the isothermal heat treatment of the Ni-B coatings.

Longabucco and Nowill [2] reported some depletion of the boron in the coating during heat treatment, but could not explain why this occurred. Also, limited attention has been paid to variation in hardness with depth into the coating. The goal of this thus is determine how phase composition and microhardness vary with depth into the coating, to determine the cause of the boron loss during heat treatment, and to examine the diffusion between the coating and a steel substrate.

2. Literature Review

2.1 Electroless Ni-B Coatings

Electroless nickel-boron coatings have long been studied as a method of improving friction and wear properties of various substrates. [4] One of the more recent developments, UltraCem (produced by UCT Coatings, Inc.), has demonstrated hardness values greater than nickel-phosphorus coatings and comparable to hard chrome coatings. UltraCem, which contains 5-6% boron by weight, has a hardness of H_{v100} 650-700 in its mostly amorphous as-plated condition. With proper heat-treatment, however, this hardness can increase as high as H_{V100} 2000, though this can take in excess of 30 weeks. [4] Briefer, more practical heat treatments can still produce hardness values of about H_{V100} 1200, allowing a useful hardness to be achieved by industrial production. [4]

2.2 Previous Work on Heat Treatment of Ni-B Coatings

Because UltraCem is a relatively new technology, the details of the transformations that take place during heat-treatment are not yet fully understood. For this reason, Longabucco and Nowill [2] heat treated samples of UltraCem plated on 1018 steel at a variety of temperatures and durations.

Microhardness measurements from the coating were collected, as well as optical and scanning electron micrographs of the coating cross-section, EDS spectra from various depths in the coating, and XRD scans of the coating surface.

Longabucco and Nowill reported that for samples heat treated for one hour at 850ºC, some delamination and some coating failure occurred. Because of this, no heat

treatments were conducted for longer than one hour at 850ºC. Heat treatments at temperatures above 850ºC were not performed.

The data collected by Longabucco and Nowill indicate that the UltraCem, which is amorphous as-deposited, crystallizes during heat treatment, forming γ-Ni and Ni_3B. [2] Much of the γ-Ni formed at the outer surface of the coating, indicating some boron depletion at the surface, which was attributed to oxidation of the boron.

Their hardness data showed, at most temperatures, an increase toward a peak hardness, followed by a decline. At the lowest temperatures, the highest hardness values came from the longest heat treatments, suggesting that longer heat treatments may have followed the same pattern as the higher-temperature heat treatments but required more time to achieve maximum hardness. The highest-temperature heat treatments showed a peak hardness at the shortest heat treatment, or no peak at all, suggesting that the transformation was occurring very rapidly.

Microscopy and EDS showed diffusion of iron from the substrate into the coating, but no detectable diffusion of nickel from the coating into the substrate. This, they suggested, led to Kirkendall porosity, which then contributed to the high-temperature coating failure. [2]

However, most of the measurements made by Longabucco and Nowill were not taken over a range of depths in the coating. Diffraction data were only obtained at the coating surface, while microhardness values were determined from averages of many measurements made at unspecified depths into the coating. From these data alone, it is not possible to accurately gauge how phase composition and mechanical properties (such as hardness) vary with depth in the coating. Because the EDS equipment used was

unable to detect boron, there is no indication of the extent of boron depletion in the coating. Finally, the question of what happened to the missing boron was not examined in depth.

2.3 Iron-Nickel Diffusion

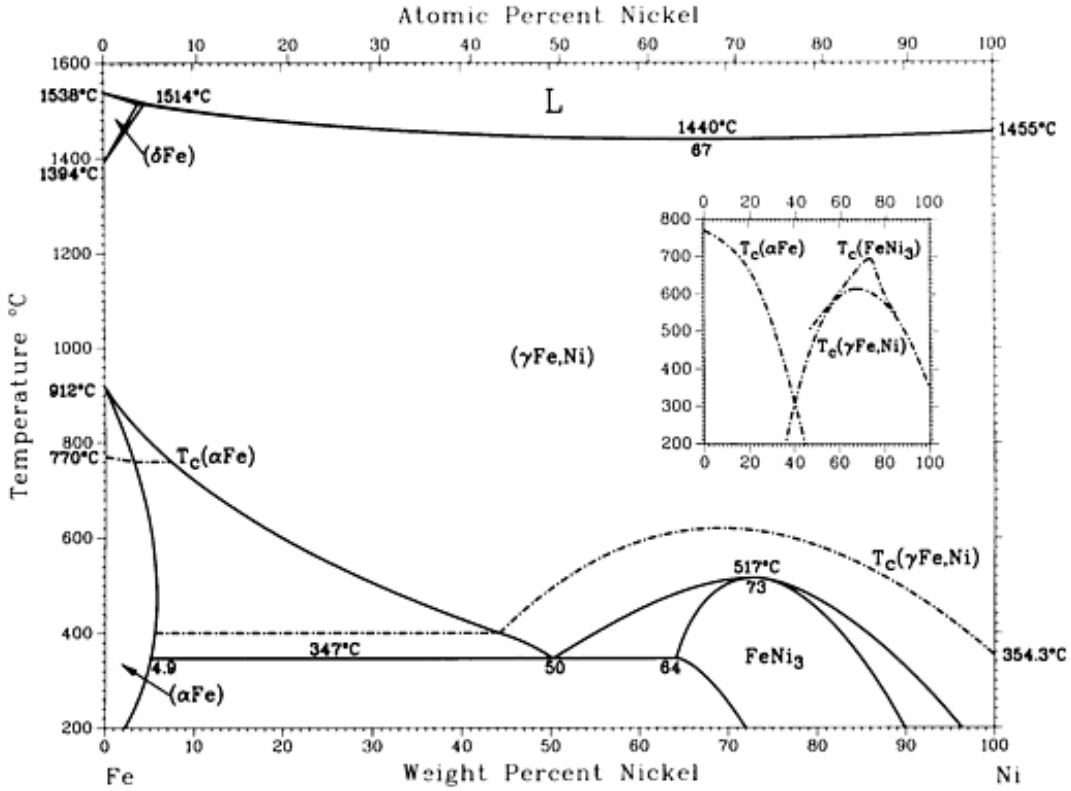

Figure 2.1: Fe-Ni phase diagram, from Swartzendruber et al. [5]

Work on the interdiffusion of iron and nickel has largely focused on temperatures above those at which this study's samples were annealed. Some data are available, however, for the temperature range in which the samples for this study were annealed.

Ustad and Sørum [6] determined iron-nickel interdiffusion coefficients at several temperatures, ranging from 635 ºC to 1325 ºC. Based on these data, they calculated activation energy and frequency factor values at 10 at% composition intervals in the iron-

nickel system. They reported activation energy values from 2.64 to 2.74 eV (approximately 255 to 264 kJ/mol) and frequency factor values from 0.15 to 0.71 cm^2/s.

Ganesan et al [7] reported that iron-nickel diffusion couples annealed at temperatures from 1073 K to 1373 K showed "smooth variations of" iron and nickel concentrations across the interface, and that interdiffusion coefficient values below 1173 K were significantly higher than predicted values based on extrapolation of higher-temperature data. Activation energy values from 310.53 to 350.06 kJ/mol and frequency factors from 174 to 2850 cm^2/s were also reported.

2.4 Boron Oxidation

Wang et al [8] found that pure solid boron, whether amorphous or crystalline, forms $B_2O_3(s)$ when exposed to oxygen at elevated temperatures up to approximately 1100 K. Above 1100K, they noted that the oxide tends to desorb from the surface as primarily $B_2O_2(g)$, which does not form during lower-temperature oxidation, with a small amount of $B_2O_3(g)$ also desorbing. They also concluded that the B_2O_3 formation resulted in submonolayer coverage, which indicates that very little oxide actually forms, even on a surface of pure boron. In addition, B_2O_3 is water-soluble, so what little oxide does form is likely to be dissolved by quenching in water.

3. Experimental Plan

Heat Treatment		Sample	
Temperature (ºC)	Time (h)	Microscopy	Diffraction
500	5	1A	1B
600	2	2A	2B
600	5	9A	9B
700	2	10A	10C
700	5	4A	4B
800	2	6A	6B
N/A	N/A	7A	7B

Table 3.1: Heat treatment and designation for original samples.

Sample	Position	Quench
8	Between	Water
11	Top	Water
12	Top	Air
13	Between	Air

Table 3.2: Conditions for new heat-treatment tests.

4. Experimental Procedure

4.1 Sample Selection

In order to ensure that comparable samples would be used for both diffraction and microscopy, several of the heat-treated samples were cut into two pieces. The heat treated samples, as well as an additional as-plated sample, were assigned designations as shown above in Table 3.1. The sample designated 10C is the reverse side of sample 10B, used because the files containing the diffraction data for sample 10B were corrupted, and the measurements thus had to be repeated.

4.2 Microscopy and Microhardness

Cross-sections were mounted in epoxy. The surfaces to be examined were ground flat using wet SiC sandpaper of progressively finer grit. They were then polished with an oil-based 3 μm diamond suspension in a vibratory polisher, followed by manual polishing using colloidal silica.

A series of photomicrographs at magnifications of 5x, 10x, 20x, 50x, and 100x were taken of each cross-section, as were scanning electron photomicrographs of the coating cross-section at 500x and at 2000x (for selected samples) of the coating surface and coating-substrate interface.

Microhardness measurements were taken at varying depths using a Knoop indenter (25 gf, 10s). The microhardness measurements and corresponding depths into the coating were used to develop a microhardness profile for each sample. In the case of Sample 10A (700ºC, 2h), additional measurements were taken in the areas of the coating with a mottled appearance.

4.3 X-Ray Diffraction

XRD was conducted at the coating surface. The sample was then carefully ground parallel to the surface to remove approximately 3-10 μm of the coating per grind, with XRD conducted at each depth. The results were, after background subtraction, analyzed by the direct comparison method to determine the relative volume fraction of all crystalline phases present. These data, along with the associated depth measurements, were used to generate a phase composition profile of each sample.

4.4 Heat Treatment and Oxidation

To examine whether the boron in the coating formed a solid oxide during heat treatment, four untreated samples were mounted as diffraction samples, and ground smooth using 600 grit SiC sandpaper. The mountings were then removed, and the samples were cleaned, photographed, and weighed. For the designations of these samples and the specific conditions of their heat treatments, see Table 3.2. All heat treatments were carried out at 800ºC for two hours.

In the heat-treatments of the original samples, a pair of stainless steel blocks were stacked inside the furnace. After these blocks had come up to temperature, the samples were placed between them, so that the samples would come up to temperature as quickly as possible. At the end of the original heat-treatments, the samples were removed from the furnace and immediately water-quenched. [2]

The first heat-treatment was designed to replicate the parameters of the original heat-treatment as closely as possible. Two samples were used: One sample was placed

between the blocks as in the original heat-treatment (indicated by "Between" in Table Foo2), while the second was placed on top of the upper block ("Top"), with its smooth face exposed to the air in the furnace, to allow for greater airflow over the surface being investigated. Both samples were placed in the furnace at approximately 800 ºC for two hours. They were then water-quenched, dried, photographed, and weighed.

Because of the possibility that any oxide(s) that had formed were water-soluble, a second pair of samples was heat-treated. This heat-treatment followed the same procedure as described above, except in that the samples were removed from the furnace and allowed to air cool. As before, the samples were then photographed and weighed.

After the above experiments, the smooth surfaces of the four heat-treatment samples were examined by X-ray diffraction, to identify the phases present.

4.5 Etching and EDS

Heat treatment sample 12 (800 ºC, 2h, air cool) was cut. Both halves were then mounted in cross-section and polished (as described earlier).

Each half of Sample 12 was etched differently. Sample 12A was etched with nital, in order to more clearly reveal the microstructure of the steel substrate. This was done to investigate whether the substrate microstructure showed any effects from the heat treatment and/or interaction with the coating. Selected areas of this sample were then examined by optical microscopy. This sample was also examined by SEM, and EDS spectra were taken at multiple locations across the substrate-coating interface. The results were used to generate concentration profiles for iron and nickel in the interface region of the sample.

To display the microstructure of the coating, Kalling's waterless (also known as Kalling's #2) reagent was used first to etch Sample 12B, but examination by SEM showed that the results were not satisfactory. The nitric/acetic acid solution used by Longabucco and Nowill [2] was then applied to the cleaned sample, which produced more satisfactory results.

5. Results and Discussion

5.1 Microscopy

5.1.1 Photomicroscopy

For the complete set of photomicrographs, see Appendix A1.

The columnar structure of the as-plated coating is visible below in Figure 5.1, as are a number of pores along the coating-substrate interface.

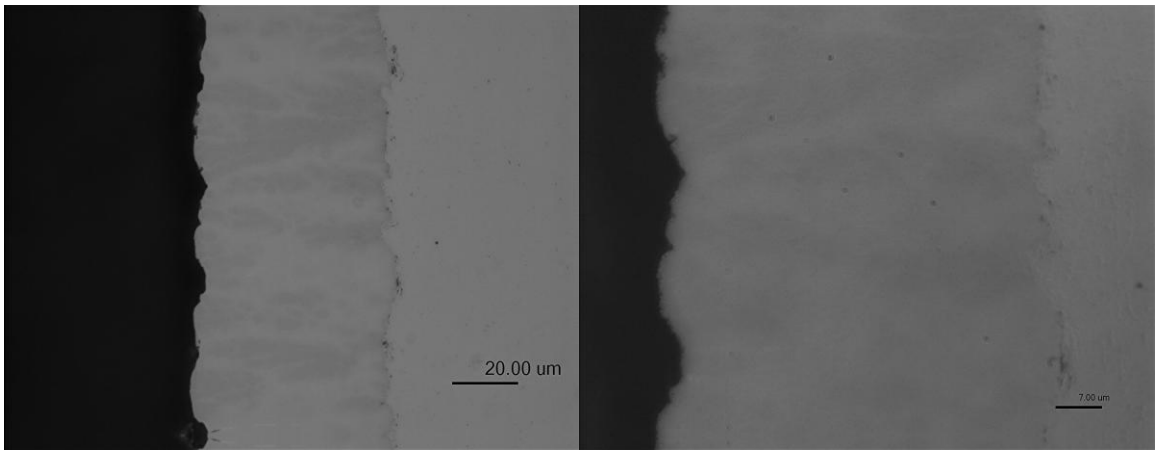

Figure 5.1: 50x (left) and 100x (right) cross-section photomicrographs of sample 7A (no heat treatment)

Coating delamination resulting from higher-temperature heat treatments was already a documented phenomenon, and separation can be clearly seen in Figure 5.2. Also visible in Figure 5.2 is the development of visually lighter layers at the coating surface and coating-substrate interface, and of some mottled areas. These mottled areas appear larger and more common closer to the surface of the coating, becoming more smaller and more scarce as one moves deeper. Microhardness, EDS, and X-ray diffraction analysis (described in later sections) suggest that the lighter areas are composed primarily of nickel-based FCC phases. Cracks perpendicular to the plane of the coating, such as the one shown in the micograph, were also observed. Pores similar

to those observed at the substrate-coating interface can be seen within the lighter interdiffusion layer.

The thickness of the surface and interdiffusion layers was measured for each sample. These measurements are summed up in Figure 5.3. As would be expected, thickness of both the surface and interdiffusion layers increases with both temperature and duration of heat treatment. Interdiffusion layer thickness is given as zero where no interdiffusion layer was visible or measurable in photomicrographs.

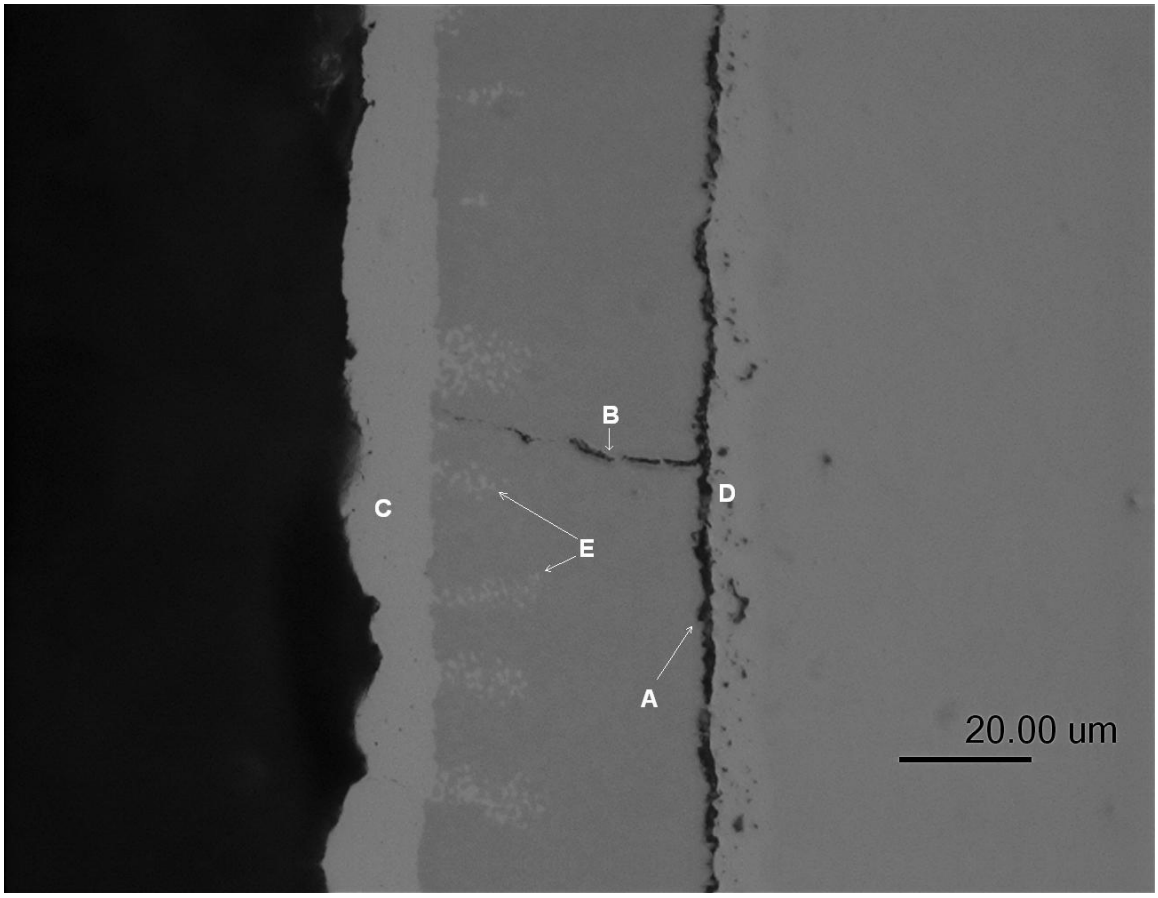

Figure 5.2: 50x photomicrograph of the cross-section of sample 6A (2 hours at 800 ºC) showing delamination (marker "A"), cracking (B), lighter surface layer (C), lighter interdiffusion layer (D), and mottled areas (E)

Sample	Time (h)	Temp (ºC)	γNi Depth (µm)	Interdiffusion (µm)
1A	5	500	2.41	N/A
2A	2	600	3.38	N/A
9A	5	600	10.14	1.86
10A	2	700	10.00	4.55
4A	5	700	13.03	5.31
6A	2	800	12.13	6.53

Table 5.1: Surface and interdiffusion layer thicknesses. Entries marked N/A indicate the absence of a visibly distinct interdiffusion layer.

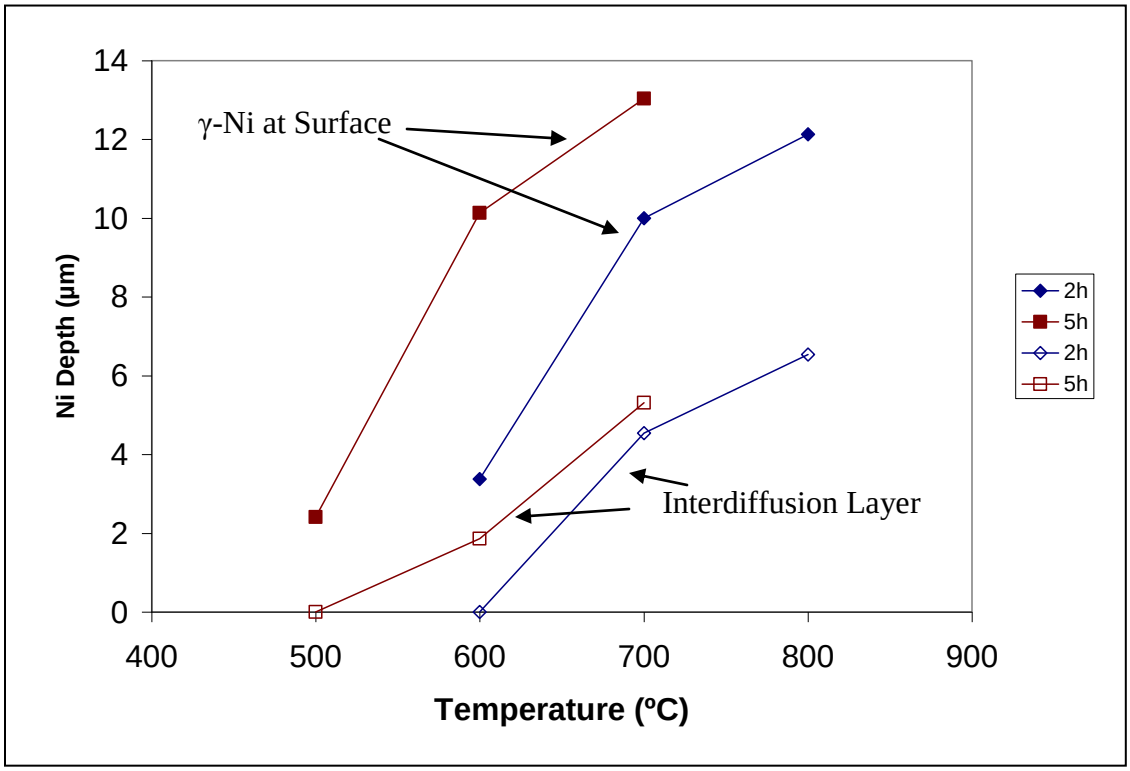

Figure 5.3: Surface and boundary layer thicknesses by anneal temperature. Solid markers are used for surface layers, open markers for interdiffusion layers.

The etching of Sample 12A revealed that the ferrite grains near the substrate-coating interface were larger than those deeper into the steel substrate. This can be clearly seen in Figure 5.4 below. A likely cause for this is grain growth during heat treatment, facilitated by diffusion of carbon out of the substrate.

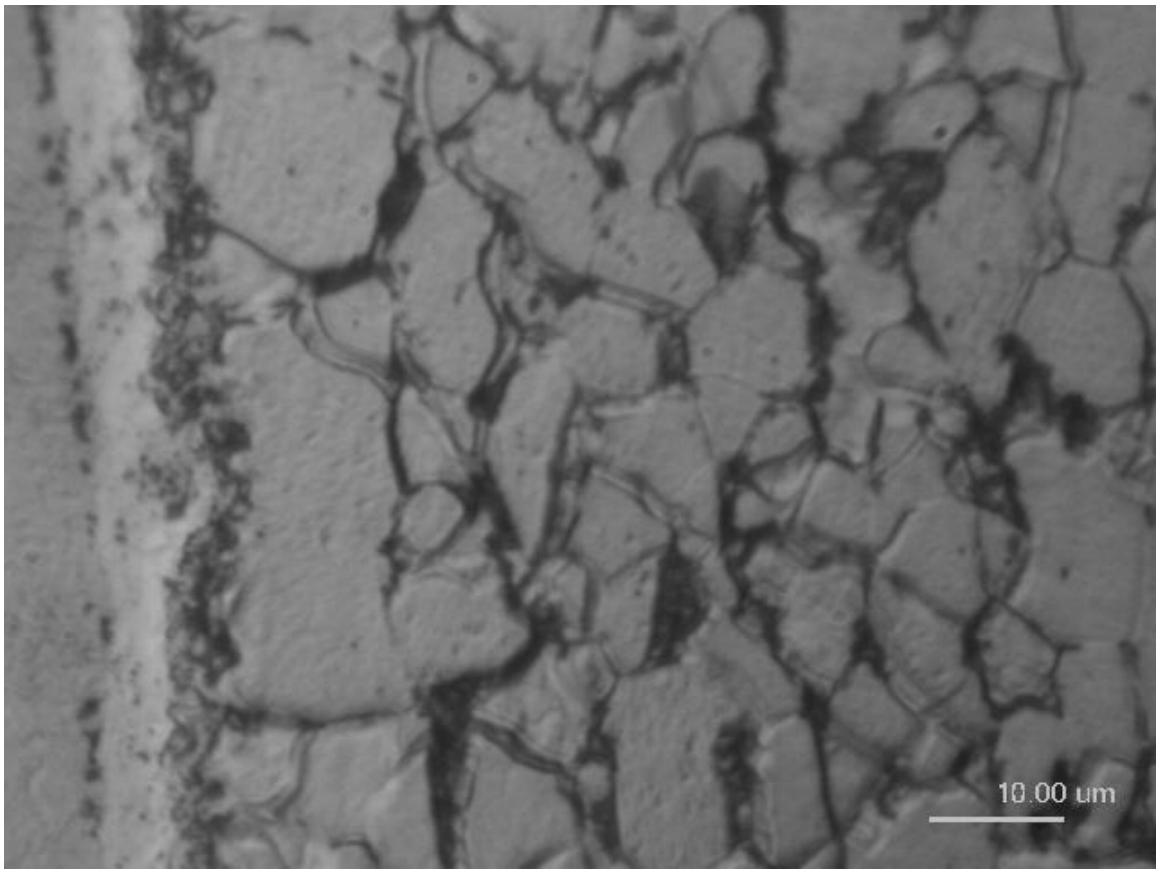

Figure 5.4: Photomicrograph of Sample 12A after etching, showing enlarged ferrite grains (immediately to the right of the interdiffusion layer) in the substrate. 100x magnification.

5.1.2 Scanning Electron Microscopy and EDS

For a complete set of scanning electron photomicrographs and EDS spectra, see Appendix A2.

A closer image of pores at the coating-substrate interface in an as-plated sample is shown in Figure 5.5 below. This image also shows the as-plated structure of the coating in more detail.

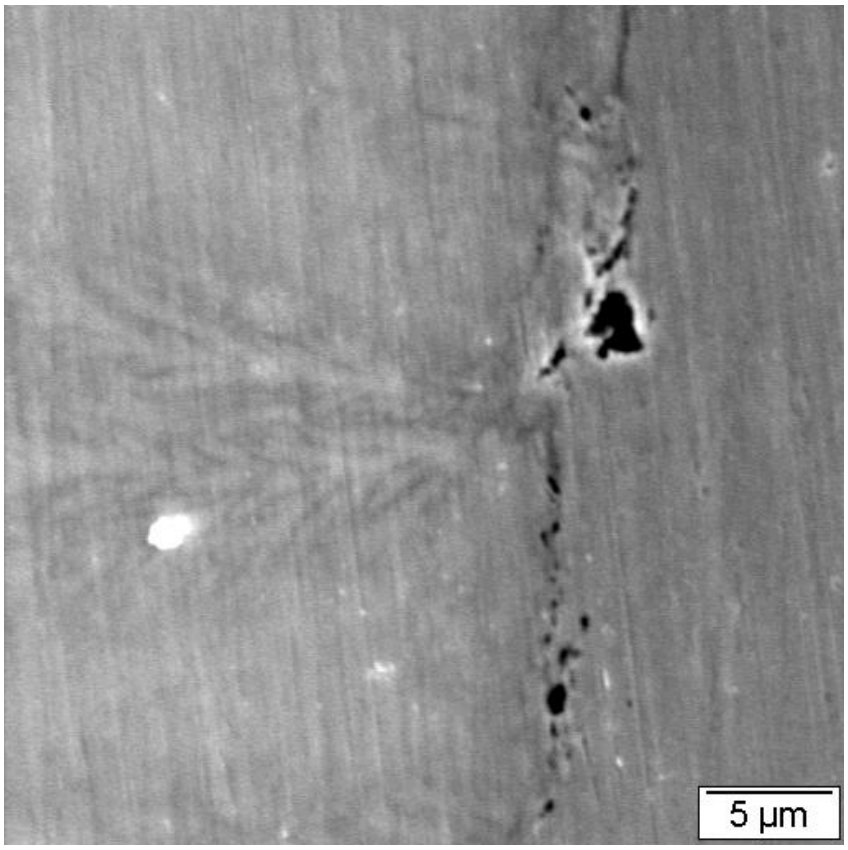

Figure 5.5: SEM micrograph of the coating-substrate interface in an as-plated sample from Longabucco and Nowill [2]. Coating is on the left.

During the grinding down of sample 6B, sections of the coating broke away, starting during the 9th grind (around 62 µm depth). SEM images were taken of delaminated areas, and EDS spectra were taken of both delaminated areas and areas that had remained intact. One of the images is shown in Figure 5.6, and the EDS spectra are shown in Figures 5.7 and 5.8.

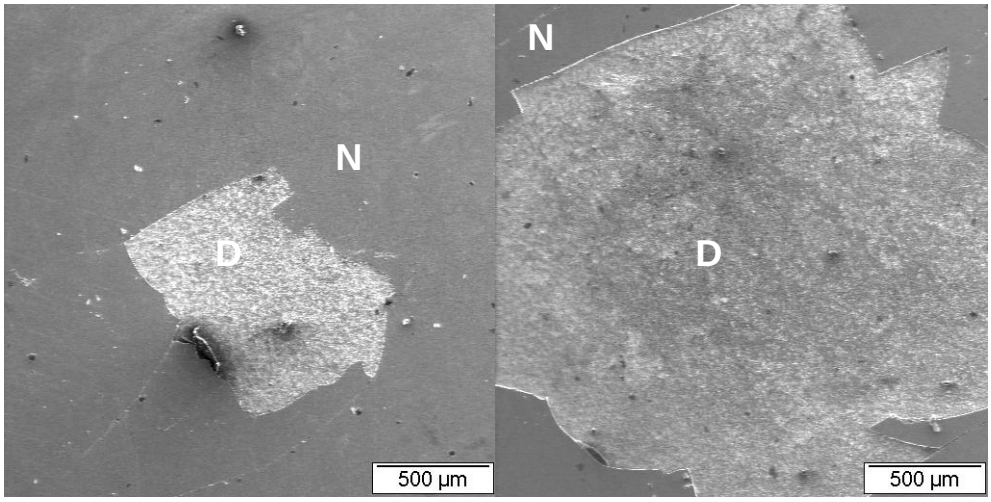

Figure 5.6: SEM micrograph of delaminated sections of sample 6B, 50x magnification. "D" indicates delaminated area, "N" non-delaminated.

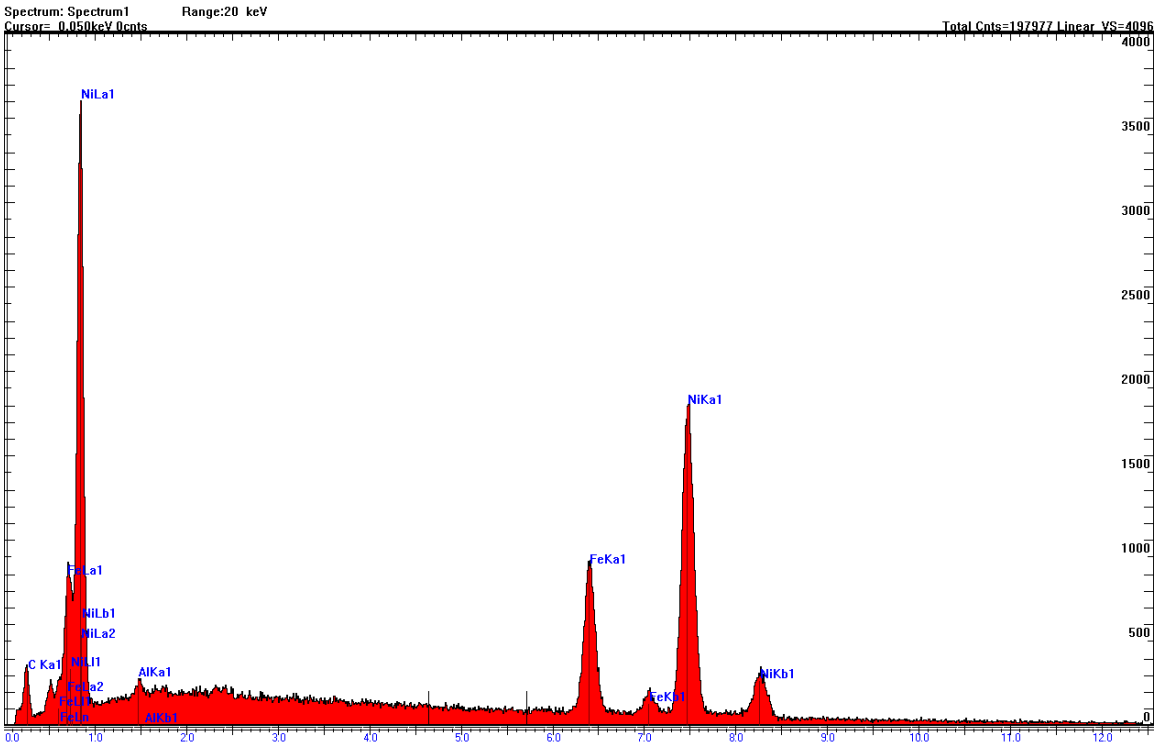

Figure 5.7: EDS spectrum of delaminated area

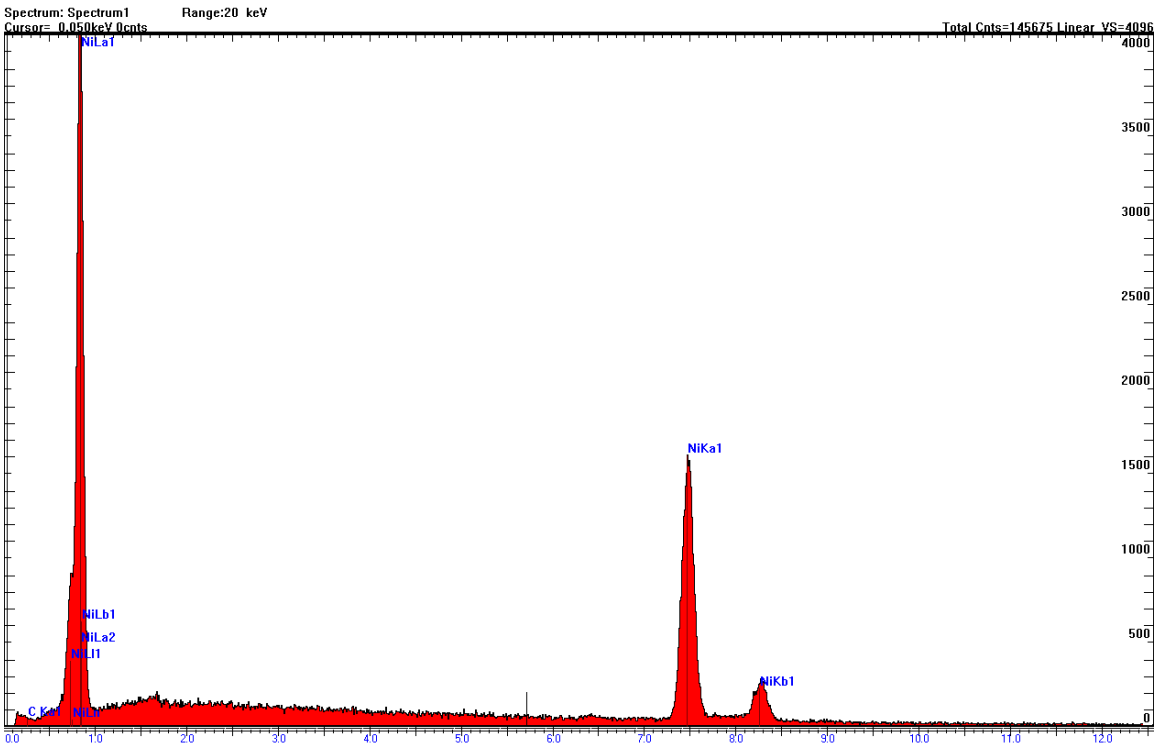

Figure 5.8: EDS spectrum of non-delaminated area

The spectrum of the non-delaminated area of the coating shows only nickel peaks. This is consistent with the XRD and other results, all of which show that at this depth, the only phases present should be γ-Ni and Ni_3B. Because boron is not detectable by EDS, the only element detected should be, and is, nickel.

In contrast, the EDS spectrum of the delaminated area shows both iron and nickel, indicating that failure has occurred within the Fe-Ni interdiffusion zone. Figure 5.2 shows failure occurring at the outward edge of the interdiffusion layer. This suggests that the interdiffusion layer is composed of a Fe-Ni alloy.

Shown in Figure 5.9 are the relative concentrations of iron and nickel plotted in front of an SEM image of Sample 12A with the position of each EDS spot marked. One notable feature in this image is that point H, in the most heavily-etched area, is the first to show pure iron, as would be expected.

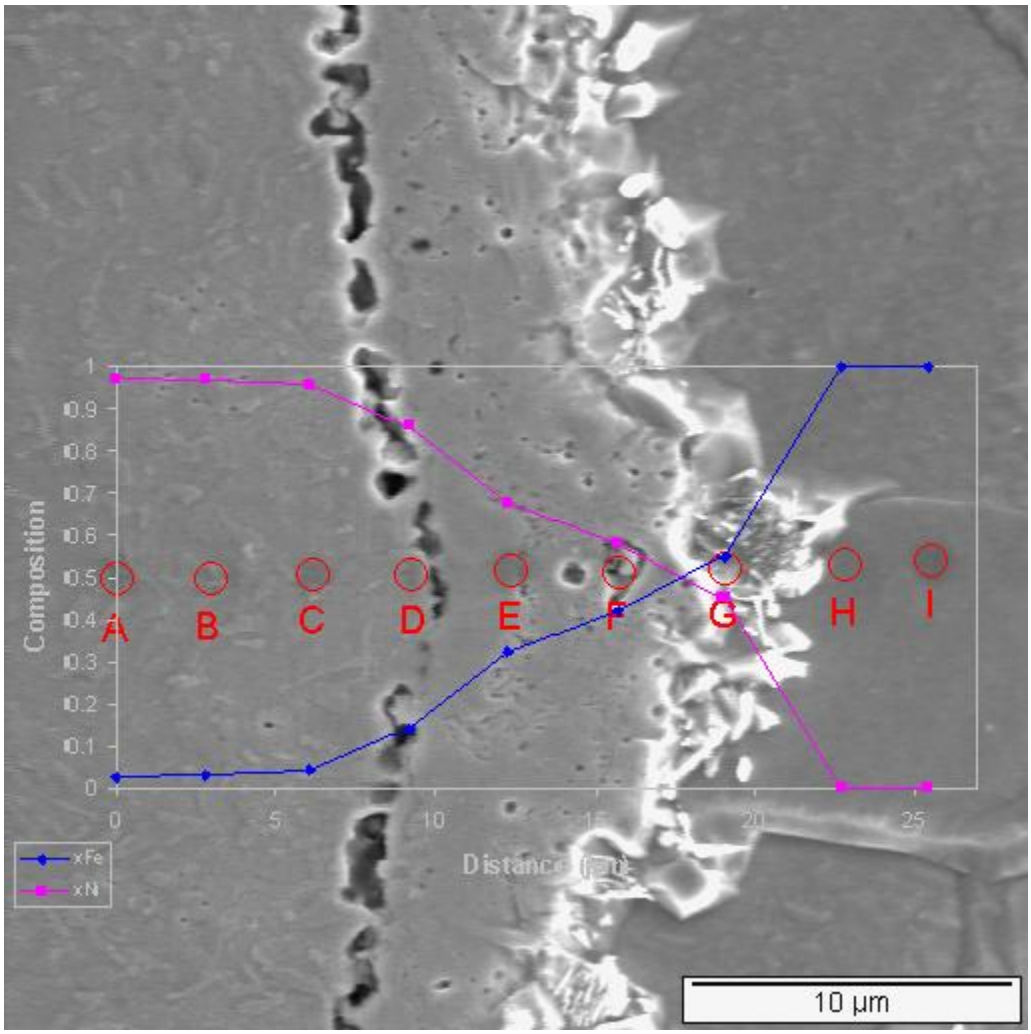

Figure 5.9: Iron and nickel concentrations in the interdiffusion area of etched Sample 12A.

5.2 Microhardness Profiles

Microhardness measurements of the samples showed significant differences between visually distinct areas of the sample. As is shown in Figure 5.10, both the surface and interdiffusion layers of the coating are significantly softer than the bulk of the coating, the darker areas of which appear to be composed entirely of Ni_3B. The coating bulk, as would be expected given the purpose of the coating, is very hard compared to the steel substrate.

(a)

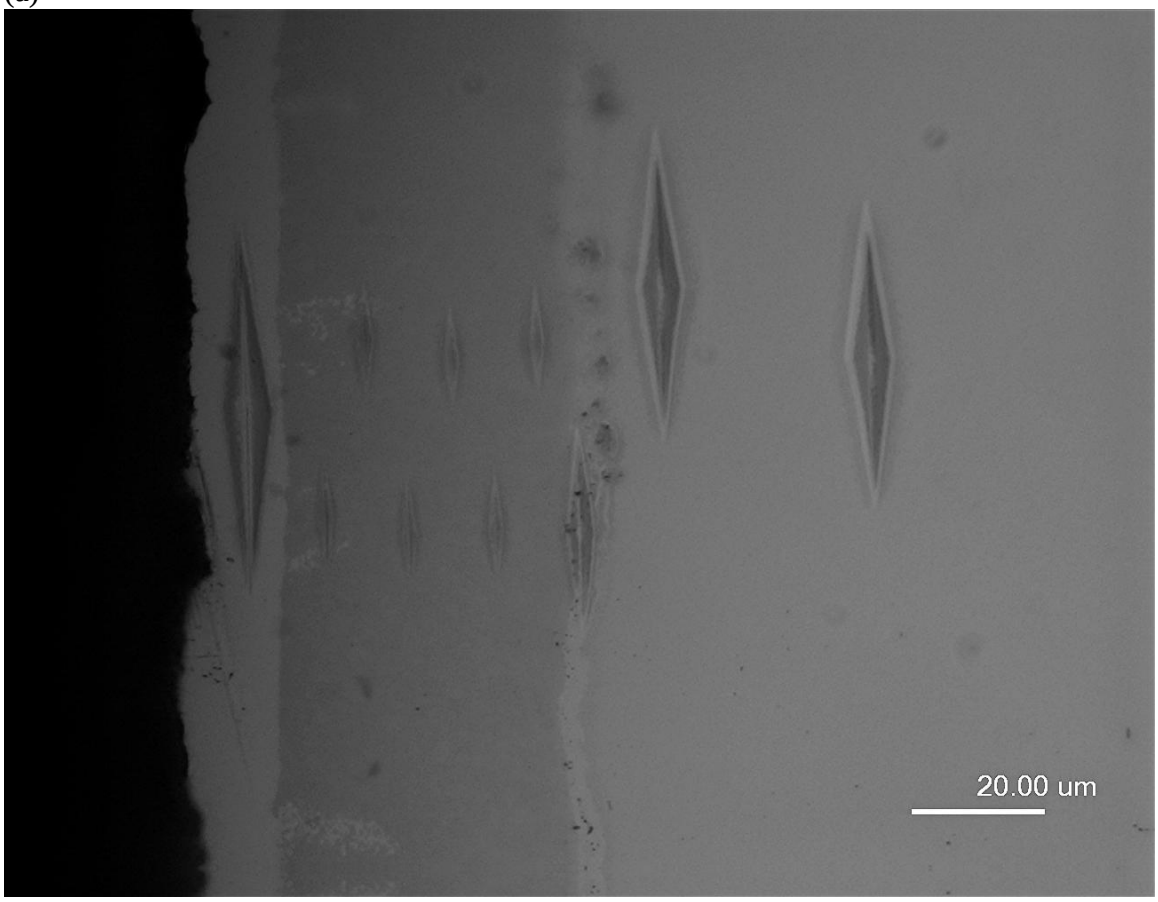

(b)

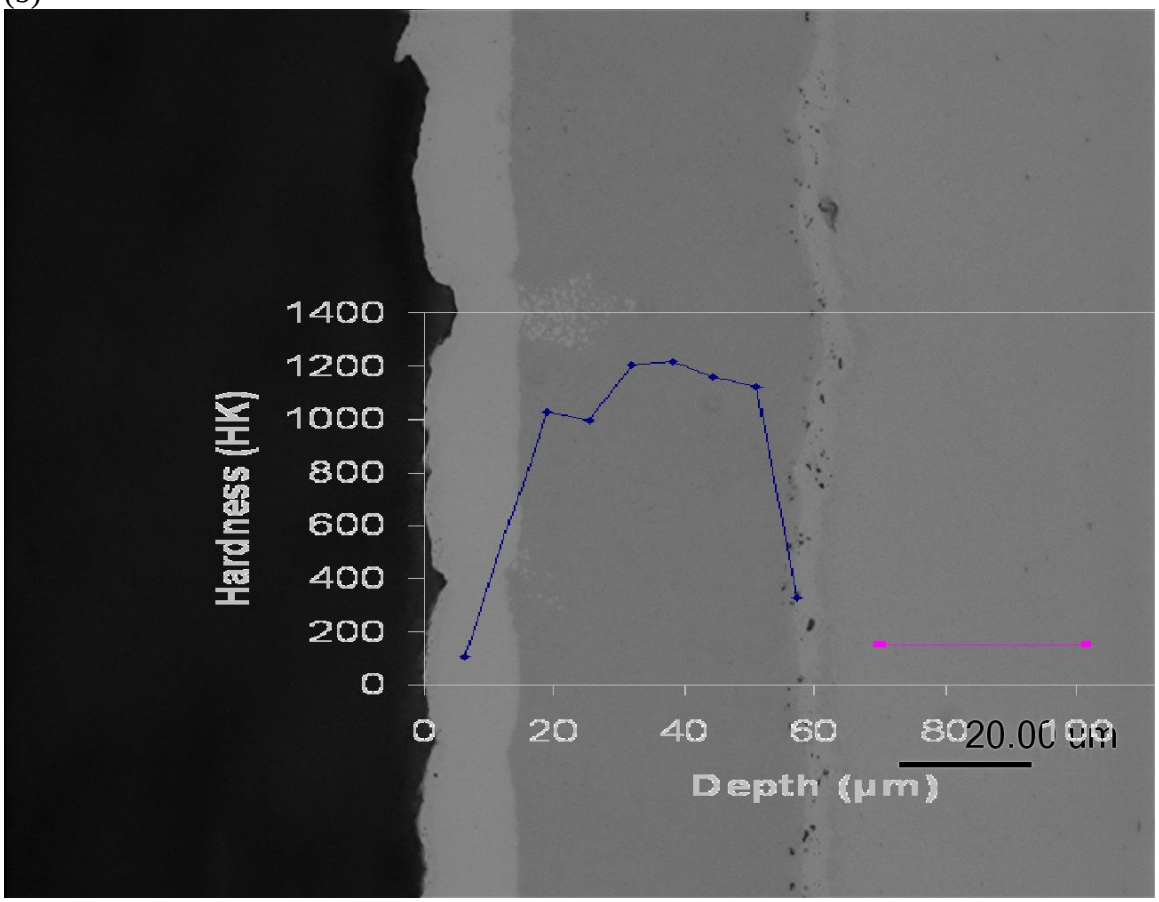

Figure 5.10: Optical photomicrographs of Sample 4A, 50x magnification; (a) Showing locations of hardness measurements. (b) Hardness profile overlay.

To investigate the nature of the mottled areas, additional hardness measurements were taken on Sample 10A within the mottled areas. Below, Figure 5.11 shows the results. The hardness in the mottled areas is markedly lower than that in the dark areas, but higher than that in the light areas. This, taken with XRD results (next section), suggests that the mottled areas are two-phase γ-Ni / Ni_3B regions.

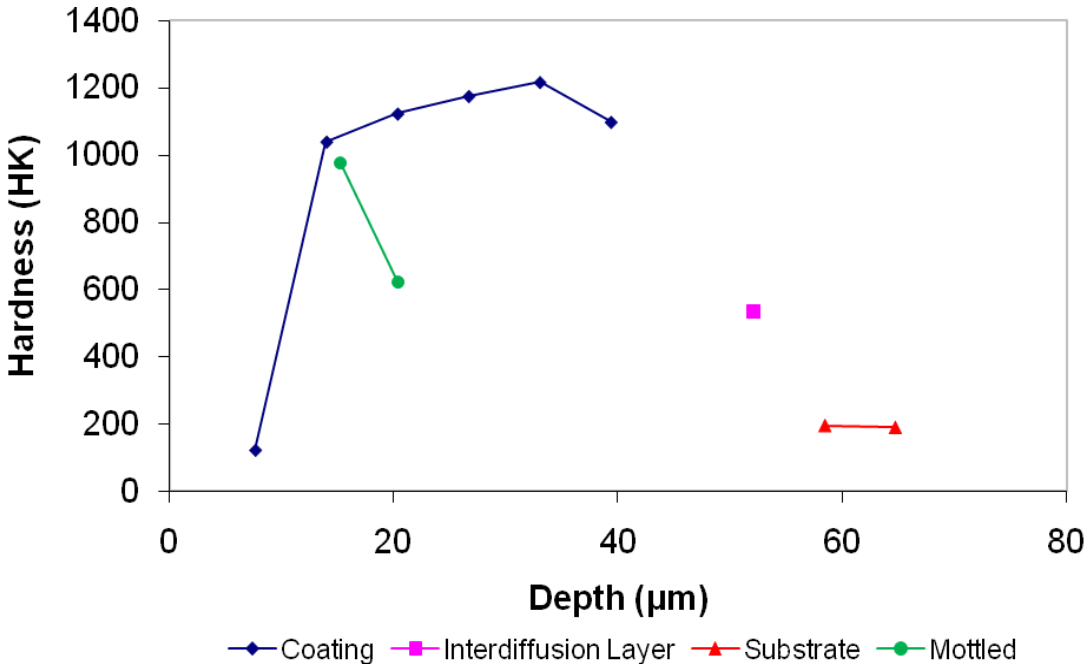

Figure 5.11: Microhardness profile for Sample 10A. The green profile is of measurements made in (on the right) or partially in (left) mottled areas.

The highest microhardness value measured for each sample is presented in Table 5.2. These results agree qualitatively with those found by Longabucco and Nowill [ditto], except that these results show no difference in maximum hardness between the two samples heat treated at 700 ºC, while Longabucco and Nowill found that hardness was greater at two hours than at five hours. It is likely that this difference stems from differing techniques: Longabucco and Nowill averaged several microhardness measurements for each sample, but do not make clear where within the coating measurements were taken. Also, as noted by Longabucco and Nowill, the small size of the indentations, especially in the coating bulk, makes exact measurement extremely difficult, resulting in a relatively large margin of error.

Sample	Time (h)	Temp (ºC)	Max HK
1A	5	500	1161.5
2A	2	600	1499.9
9A	5	600	1338.8
10A	2	700	1216.5
4A	5	700	1216.5
6A	2	800	1174.9

Table 5.2: Maximum microhardness values for each sample.

Optical micrographs showing the microhardness indentations can be found with the other optical micrographs in Appendix A1. Microhardness data, as well as additional profile overlays like that in Figure 5.9, are found in Appendix A3.

5.3 X-Ray Diffraction

Diffraction analysis of sample surfaces shows the presence of significant fractions of γ-Ni in addition to the Ni_3B that would be expected from the as-plated composition of the coating. The fraction of γ-Ni present drops rapidly with increasing depth into the sample, with the bulk of the coating composed primarily (or, for some samples, entirely) of Ni_3B. Differences in γ-Ni fraction in the coating bulk can be attributed to the variability in initial composition of the as-plated coating.

The phase composition profiles for Sample 9B (600 ºC, 5h) and 10C (700 ºC, 2h) do not show the presence of the interdiffusion layer visible in the micrographs of their corresponding cross-section samples (See Figure 5.12 (c) and (d)). This is likely due to a combination of two factors: First, the interdiffusion layer is thinner than the typical grind depth on those samples. Second, the interdiffusion layer is, as demonstrated by microhardness measurements, considerably softer than the Ni_3B bulk of the coating. Thus, it is likely that for both Sample 9B and 10C, one of the grinds that was performed

completely removed the interdiffusion layer. Phase composition profiles and cross-sectional micrographs are shown for each sample in Figure 5.12, below. For a complete set of phase composition profiles, see Appendix A4.

(a)

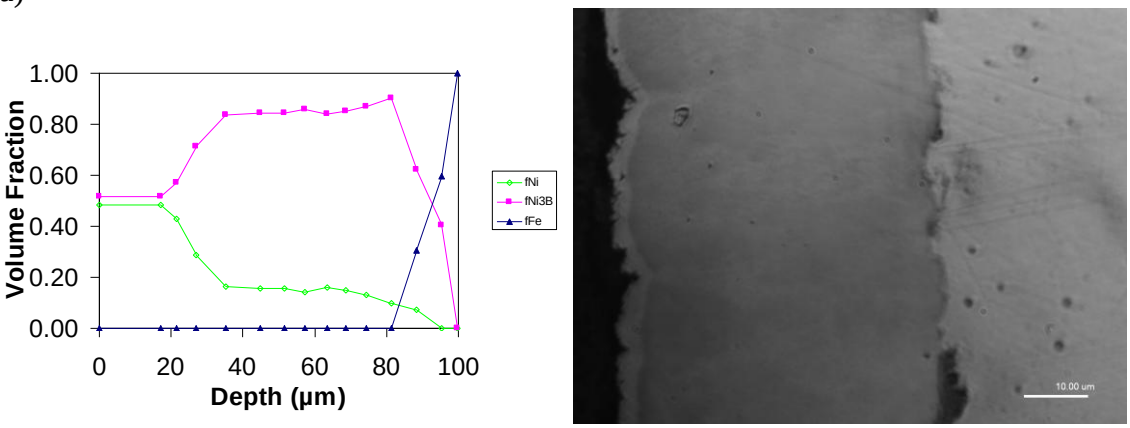

(b)

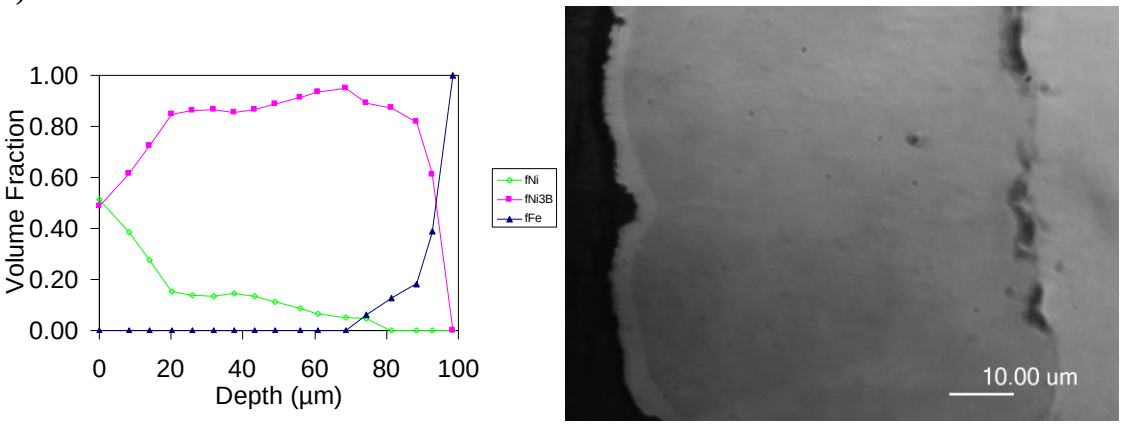

(c)

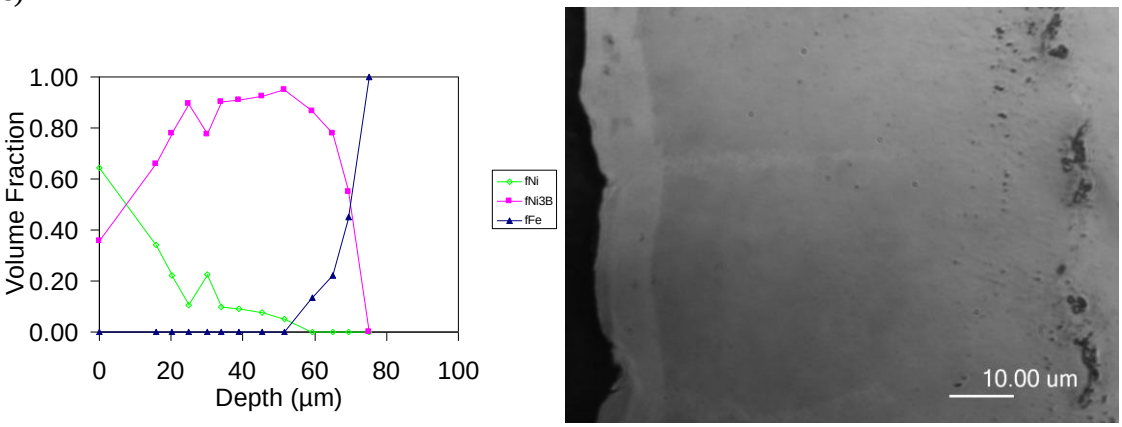

(d)

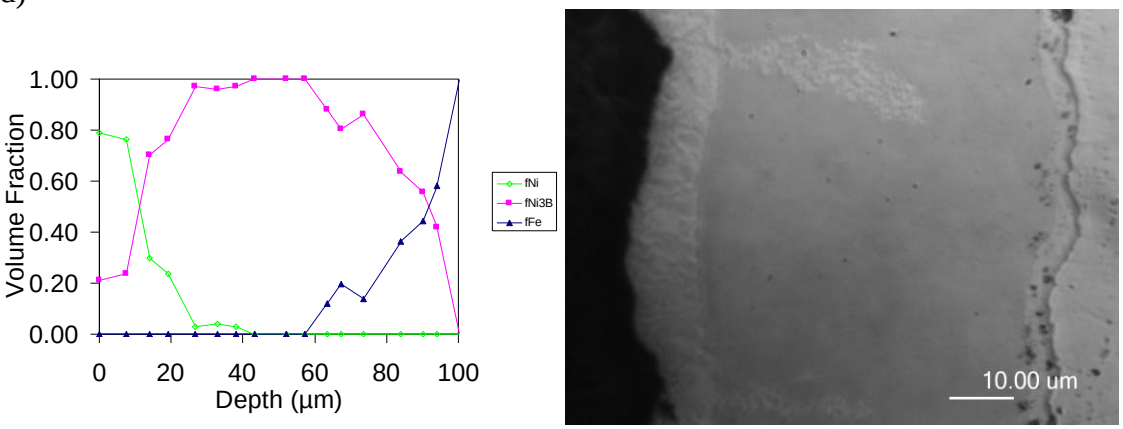

(e)

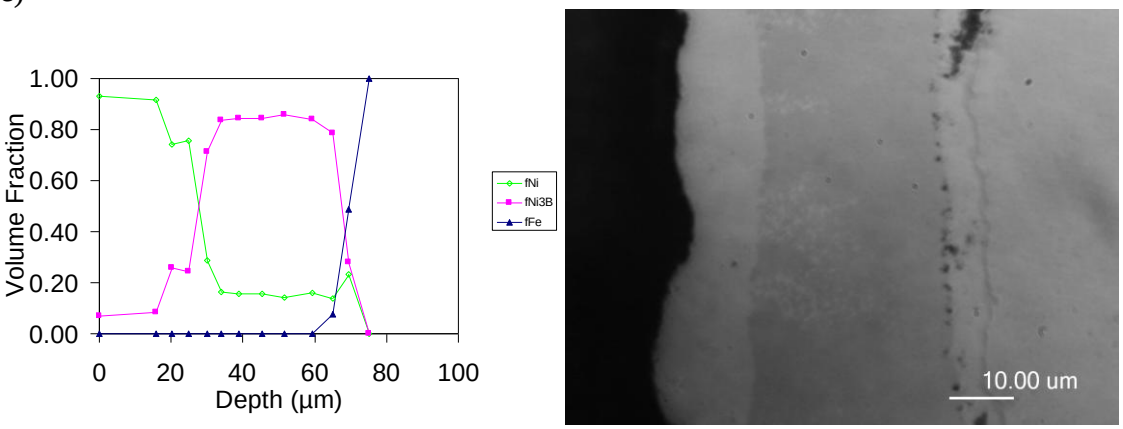

(f)

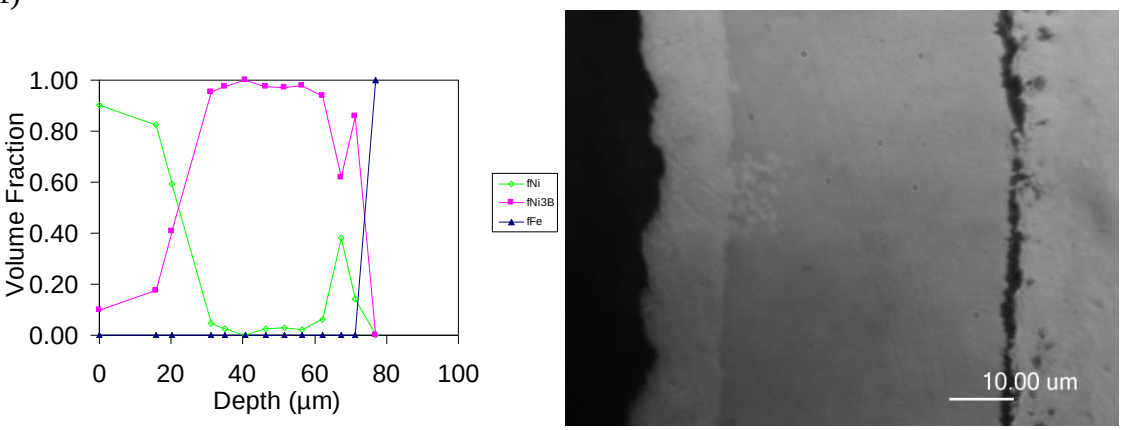

Figure 5.12: Phase composition profiles and 100x optical photomicrographs; (a) Sample 1 (500 ºC 2h); (b) Sample 2 (600 ºC 2h); (c) Sample 9 (600 ºC 5h); (d) Sample 10 (700 ºC 2h); (e) Sample 4 (700 ºC 5h); (f) Sample 6 (800 ºC 2h)

While it is highly likely that the interdiffusion layers that formed contained Fe Ni_3, the X-ray diffraction pattern of this phase is very similar to that of γ-Ni. The two phases can be distinguished using lower-intensity peaks, but this is not feasible in the

current study, as the relative intensity of background noise is very high on many of the later XRD scans.

5.4 Heat Treatment and Oxidation

The weight before and after heat treatment for each sample is shown below in Table 5.3. Both water-quenched samples showed a net weight loss, whereas both air-cooled samples showed a net weight gain. This is consistent with the hypothesis that a layer of solid B_2O_3 forms on the sample surface during annealing and is then dissolved away during the water quench.

Sample	Position	Quench	Wt. Before	Wt. After	Change
8	Between	Water	3.9163 g	3.9072 g	-9.1 mg
11	Top	Water	3.7178 g	3.7093 g	-8.5 mg
12	Top	Air	2.6195 g	2.6295 g	+10 mg
13	Between	Air	3.6749 g	3.6840 g	+9.1 mg

Table 5.3: Weight measurements and weight differences before and after heat treatment

All heat treatment samples were observed, after annealing, to have a rougher surface on the side which had previously been ground smooth. Potential contributing factors are plastic deformation caused by the crystallization of the coating and the formation of a solid B_2O_3 layer. However, the uniformity of appearance between the water-quenched and air-cooled samples suggests that the change in surface finish was not due to the presence of B_2O_3 on the sample surface.

Cross-sectional microscopy of sample 12 showed a considerably thicker γ-Ni surface layer on the side of the coating not in contact with the stainless steel block during annealing, as shown below in Figure 5.13. Also of note is the absence of cracking between coating and substrate on the left (block) side of the sample. The coating would have cooled more slowly on this side of the sample, due to its greater thickness, and would have cooled significantly more slowly than the coating on the water-quenched

samples. This suggests that cooling rate of the coating plays a role in the cracking observed in samples annealed at high temperatures.

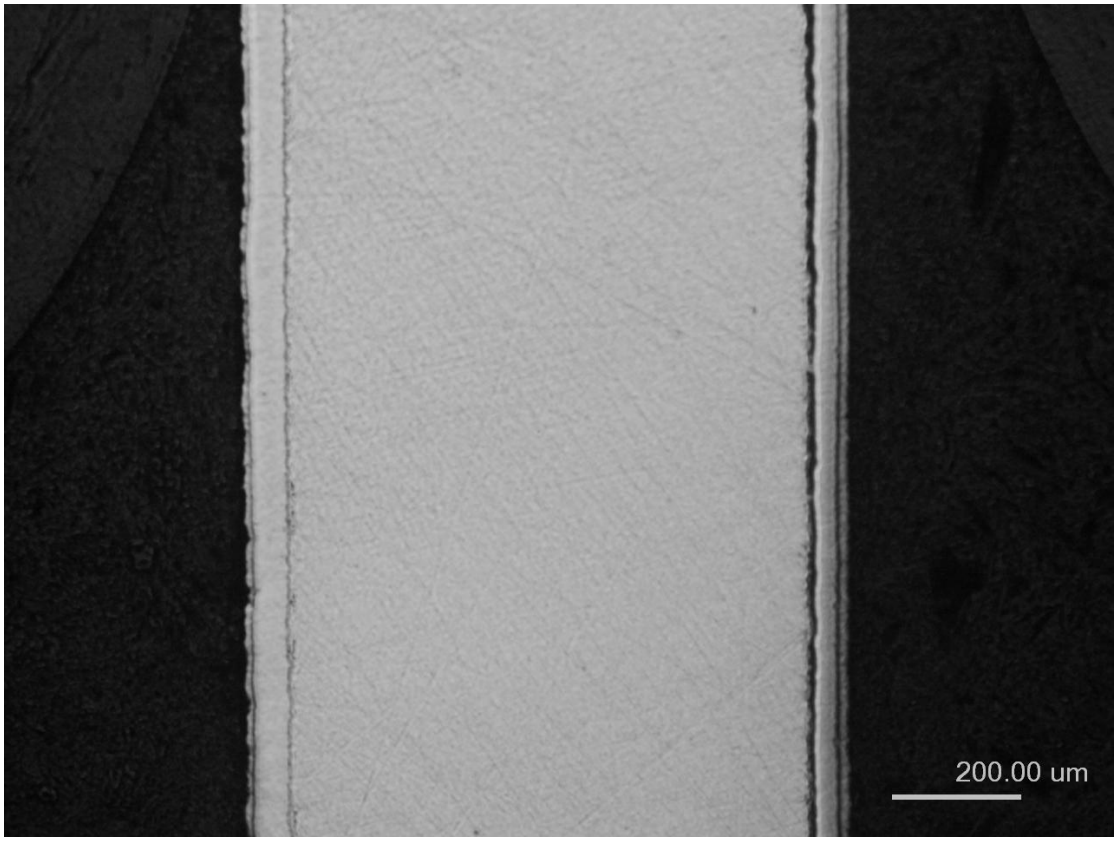

Figure 5.13: Optical photomicrograph of sample 12B (800 ºC, 2h, air cool, top). Surface to the left was in contact with stainless steel block during annealing.

The expected thickness of the B_2O_3 layer was calculated based on the thickness of the γ-Ni surface layer, which (given the initial coating composition) indicates the amount of boron lost. Using the maximum rated initial boron content (6 wt%), a B_2O_3 thickness of approximately 19 μm is predicted. This would be expected to be visible in cross-sectional samples, but several stages of the cutting, grinding, and polishing process utilized water and/or water-based coolants, lubricants, and/or polishing suspensions, which would have dissolved any oxide present before imaging. X-ray diffraction of the air-cooled samples showed a peak that could not be attributed to γ-Ni, Ni_3B, or α-Fe. This peak is consistent with the highest-intensity [310] peak of B_2O_3. [9]

6. Conclusions

During annealing, boron near the surface of the coating oxidizes to form B_2O_3(s). This results in the formation of a soft layer of γ-Ni at the sample surface.

The bulk of the coating after heat treatment is composed either primarily of Ni_3B, depending on the exact as-plated composition of the sample. Uneven distribution of boron in the as-plated coating may result in two-phase regions of γ-Ni and Ni_3Fe after annealing.

Iron-nickel diffusion between the coating and substrate during annealing leads to the development of a interdiffusion layer composed of Ni_3Fe and α-Fe. The porosity at this depth observed in previous research and attributed to Kirkendall porosity appears to be due at least in part to incomplete contact between coating and substrate prior to heat treatment.

Rapid cooling of samples annealed at higher temperatures (800 ºC and above) is a significant factor in cracking and subsequent failure of the coating observed in this work and coating failure reported in previous work.

7. Suggestions for Future Research

The roughness of the as-plated sample surfaces (and resultant roughness after heat treatment) presented a difficulty when comparing diffraction data to micrographs, as it made the exact location of the sample surface ambiguous. For this reason, it is recommended that future studies grind smooth the coating surface prior to heat treatment, in order to reduce the roughness of treated samples. In addition, care should be taken to remove any burrs or other localized deformation caused by sectioning of samples, as these can interfere with some measurements and prevent the sample from laying flat.

If possible, a method of sectioning and polishing cross sections of air-cooled samples without the use of water, so that the B_2O_3 layer can be examined by microscopy.

More detailed study of phase distribution within the coating is suggested. A more precise method of removing material from the sample is desirable, especially one which ensures that the new surface generated by material removal is flat and parallel to the previous surface. Also preferable is a more precise method of measuring the amount of material removed, in order to more reliably determine the depth within the coating at which examination is taking place.

Because stainless steel blocks were placed in direct contact with the sample surface during heat treatment, the possibility exists that diffusion may occur between these blocks and the sample. Tests should be performed with a known block composition, examining both contact and non-contact areas before and after heat treatment. If possible, these results should be compared to those generated using samples that will not experience sample-block diffusion, controlling for surface finish, to account

for the possibility that the sample simply impedes furnace atmosphere from reaching the contact area of the block.

Additional study should be done to quantify the extent of Fe-Ni diffusion between the coating and substrate, and to compare this to the degree of diffusion reported between pure iron and nickel.

8. Works Cited

[1] Riddle, Y.W., UCT Coatings, Inc. (2005) Nickel Boride (Ni_3B) Plating

[2] Longabucco, Johnathan, and Nowill, Courtney. "Phase Transformations of Ni-B Coating." Major Qualifying Project. Worcester Polytechnic Inst, 2006.

[3] Delaunois, F., Lienard, P. "Heat treatments for electroless nickel-boron plating on aluminum alloys." Surface and Coatings Technology. 160 (2002): 239-248.

[4] Riddle, Y.W., Bailer, T.O. "Friction and Wear Reduction via and Ni-B Electroless Bath Coating for Metal Alloys." JOM (2005): 40-45.

[5] ASM Handbook. Volume 3, Alloy Phase Diagrams. 10th ed. 2000.

[6] Ustad, T. and Sørum. "Interdiffusion in the Fe-Ni, Ni-Co, and Fe-Co Systems." Phys. Stat. Sol. (a) 20 (1973): 285-294.

[7] Ganesan, V; Seetharaman, V.; and Raghunathan, V.S.. "Interdiffusion in the Nickel-Iron System." Materials Letters 4.2A (1984): 257-262.

[8] Wang, Yajun; Fan, Jingfu; and Trenary, Michael. "Surface Chemistry of Boron Oxidation. 1. Reactions of Oxygen and Water with Boron Films Grown on Ta(110)." Chemistry of Materials 5.2 (1993): 192-198.

[9] JCPDS Card File. Card # 6-0297.

Appendix A1: Optical Microscopy

See file “Appendix A1.doc” on CD-ROM.

Appendix A2: SEM and EDS

See file “Appendix A2.doc” on CD-ROM.

Appendix A3: Microhardness Data and Overlays

See file “Appendix A3.doc” on CD-ROM.

Appendix A4: XRD Phase-composition Profiles

See file “Appendix A4.doc” on CD-ROM